Hindawi
Geofluids
Volume 2018, Article ID 2608435, 9 pages
https://doi.org/10.1155/2018/2608435

Research Article

A Novel True Triaxial Apparatus for Testing Shear Seepage in Gas-Solid Coupling Coal

Gang Wang,[1,2] **Pengfei Wang**,[2] **Yangyang Guo**,[2] **and Wenxin Li**[2]

[1]*Mine Disaster Prevention and Control-Ministry of State Key Laboratory Breeding Base, Shandong University of Science and Technology, Qingdao 266590, China*
[2]*College of Mining and Safety Engineering, Shandong University of Science and Technology, Qingdao 266590, China*

Correspondence should be addressed to Gang Wang; gang.wang@sdust.edu.cn

Received 1 May 2018; Revised 11 July 2018; Accepted 25 July 2018; Published 2 September 2018

Academic Editor: Simone Marasso

To study the effects of shear stress on the mechanical and seepage properties of gas-bearing coal in three-dimensional stress conditions, a novel true triaxial apparatus (TTA) was developed for the rigid loading of the major principal stress σ_1 and the intermediate principal stress σ_2, and for the flexible loading of the minor principal stress σ_3. Both the upper and lateral pressure heads do not interfere with each other when loading σ_1 and σ_2. The control and measurement of gas flow sealed effectively in coal samples were achieved by using a gas seepage system. The TTA was used to perform a series of experiments on shear seepage in coal samples under true triaxial stress conditions. The experimental results about coal's shear failure modes, shear stress-shear displacement curve, and permeability-shear displacement curve all showed that the TTA with its better accuracy and reliability had advantages in studying the effects of both the intermediate principal stress and shear deformation on the mechanical properties of coal samples and on the characteristics of gas seepage. Thus, it could provide a new test means for further studies on shear-induced seepage in the gas-solid coupling coal.

1. Introduction

Coal and gas outburst is an extremely complex gas dynamic phenomenon encountered in the production of underground coal mines and characteristic of a sudden eruption of a large amount of gas and coal towards the roadway or stope within a very short period of time [1]. When coal and gas outburst occurs, the process that coal mass is gradually damaged and thrown out from shallow to deep is mainly controlled by the distribution of stress in the mine wall as well as the tensile and shear damages induced by gas pressures in pores and fractures to the coal mass; and with these damages continuously developing, the coal mass of the mine wall becomes mainly subject to shear failure that affects coal's mechanical properties and permeability [2]. Therefore, a good understanding of the effects of shear failure on the mechanical properties and seepage characteristics of coal is important for gaining insight into the coal and gas outburst mechanism.

Coal seams prone to coal and gas outbursts are highly risky for field trials; therefore, the simulation test is an effective means to explore the mechanisms of coal and gas outburst. The compressive strength as well as the deformation and permeability of coal and rock have been studied by means of different types of conventional triaxial apparatus [3–10]. Chen et al. and Liu et al. studied the damage development and permeability in the reconstituted coal specimens during stress unloading using a coupled "mechanical-permeability" system [11, 12]. Wang et al. studied the deformation and gas flow characteristics of coal-like materials under conventional triaxial stress conditions [13].

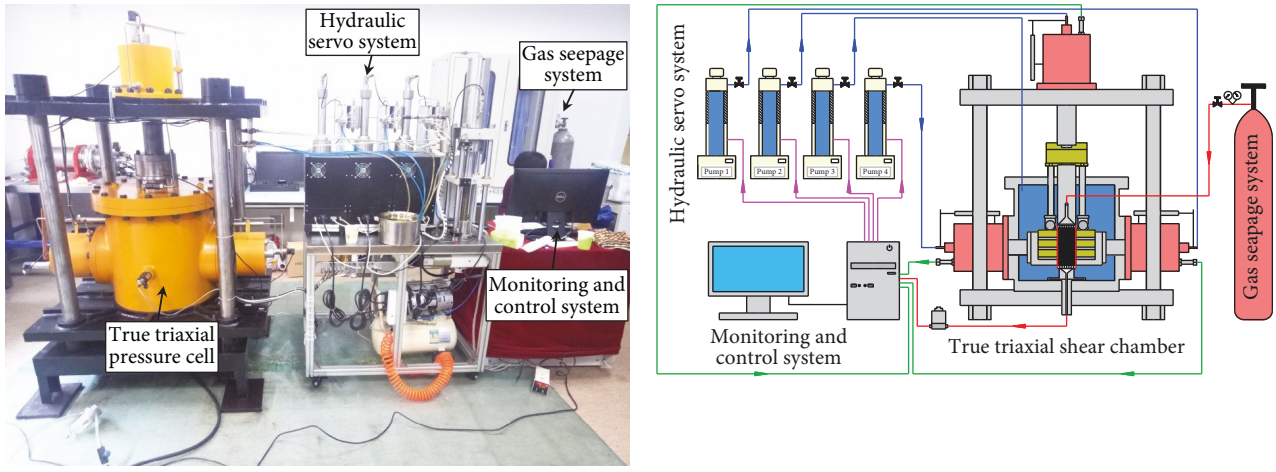

(a) Photos of true triaxial apparatus

(b) Schematic diagram of the true triaxial apparatus

Figure 1: Diagrams of true triaxial apparatus.

However, the conventional triaxial tests often neglect the effects of intermediate principal stress and cannot reflect the actual complex ground stress conditions. Therefore, many scholars have developed true triaxial apparatus and carried out a large number of compression seepage tests [14–21]. The effects of the intermediate principal stress on the mechanical properties of coal mass were explored through the true triaxial devices [22–25]. Li et al. studied the permeability evolution of shale under anisotropic true triaxial stress conditions using a self-developed multifunctional true triaxial flow-solid coupling test system [26].

In addition, a variety of shear-seepage coupling test devices have been developed to explore the effects of shear deformation on coal mechanics and seepage characteristics [27–33], which are usually limited to the liquid seepage media. Wang et al. carried out shear-fluid coupling tests for rocks under different boundary conditions using an improved numerically controlled shear-fluid coupling apparatus [34]. Xu et al. studied the evolution process of shear microcracking, expansion, and macroscopic failure of gas-containing coals under the compression-shear load condition using a self-developed microscopic shear testing device for coal rock [35]. Other scholars have combined numerical simulation with physical experiments to study the motion of microfluids in pore fractures [36–39].

Although the above-mentioned tests on coal and rocks advanced our understanding of outburst mechanisms, studies on the effect of shear failure on the mechanical properties and gas flow characteristics of coal under true triaxial stress are very rare. Thus, we independently developed a novel true triaxial apparatus for the gas-solid coupling coal shear-seepage test. Our equipment is mainly to study the mechanical properties and permeability characteristics of coal bodies under three-dimensional shear forces. That is, the primary cracks and pores in the coal body undergo compression deformation when subjected to different effective stresses, which affect the flow of the inside microfluids. In addition, the device can also study the adsorption and desorption of microfluids in the pores of coal, and its effects on the deformation, shear strength, and permeability of coal, especially methane, carbon dioxide, nitrogen, and other gases.

2. Overall Designs of the Novel True Triaxial Apparatus

The apparatus consists mainly of a true triaxial pressure cell, a hydraulic servo system, a gas seepage system, and a monitoring and control system, as shown in Figure 1. The main technical indicators are as follows: (1) specimen size: 200 mm × 100 mm × 100 mm; (2) major principal stress (σ_1) applying range 0–70 MPa, axial strain (ε_1) range 0–50 mm; intermediate principal stress (σ_2) applying range 0–35 MPa, lateral strain range (ε_2) 0–40 mm; minor principal stress (σ_3) applying range 0–10 MPa, lateral strain (ε_3) range 0–40 mm; and (3) gas pressure (P) range 0–3 MPa. The apparatus can be used for conventional triaxial and true triaxial shear and compression seepage tests of coal and rock under three-dimensional unequal stress and pore pressure conditions.

2.1. True Triaxial Pressure Cell. The true triaxial pressure cell is the core component of the apparatus providing the necessary three-dimensional stress for experimental tests and the operational basis for the in-hermetic seepage system. It contains true triaxial pressure cell frames, a major principal stress (σ_1) applying system, an intermediate principal stress (σ_2) applying system, and a minor principal stress (σ_3) applying system. Figure 2 shows the schematic diagram of the true triaxial pressure cell, and Figure 3 shows the interior structure of the true triaxial pressure cell.

2.1.1. True Triaxial Pressure Cell Frame. The true triaxial pressure cell frame is composed of an upper bracket, a lower socket, and four upright posts. The lower socket contains a circular groove where the main body of the pressure cell is embedded. Both the upper bracket and the lower socket are subjected to stiffener treatment to ensure that their frame structures have sufficient rigidity.

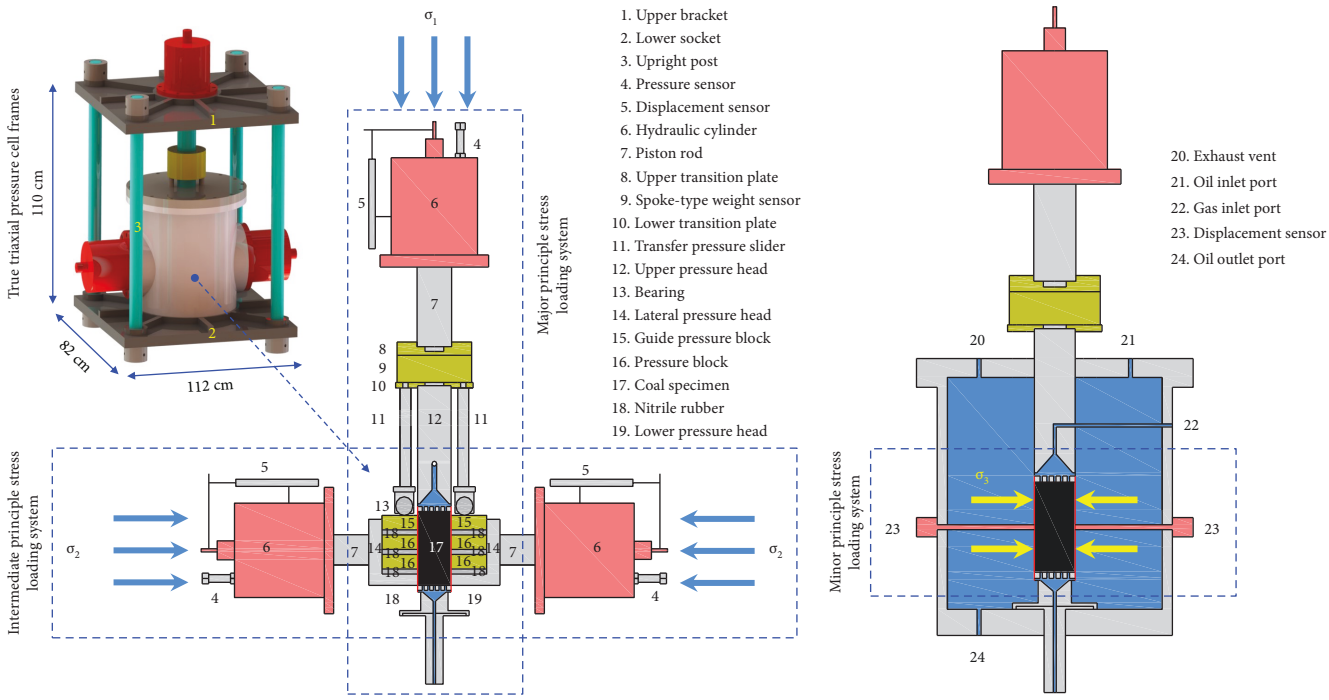

(a) Front view (b) Left view

Figure 2: Schematic diagram of the true triaxial pressure cell.

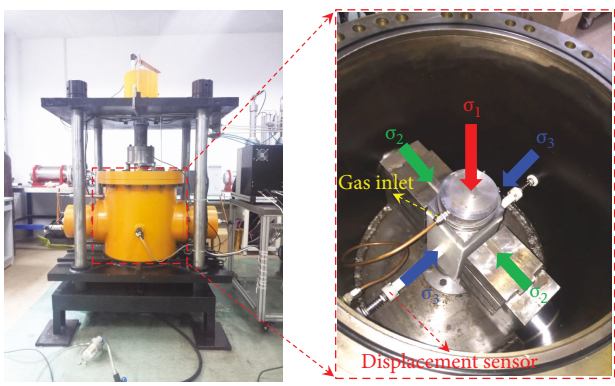

Figure 3: Interior structure of the true triaxial pressure cell.

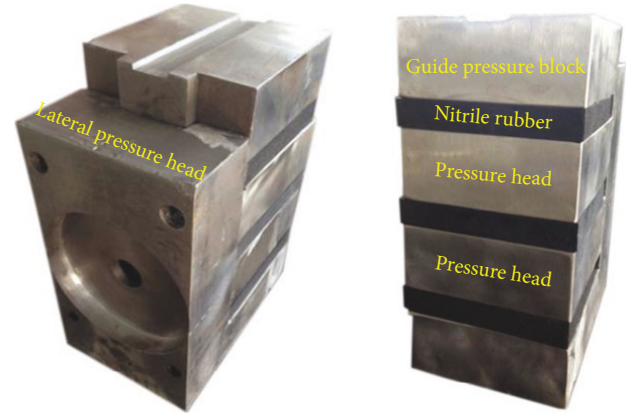

Figure 4: Lateral pressure head.

2.1.2. Major Principal Stress Applying System. As shown in Figure 2(a), the major principal stress (σ_1) applying system uses the rigid applying mode. By injecting oil into the hydraulic cylinder 6, the pressure in the hydraulic cylinder rises and the piston rod 7 is pushed downwards, so that the upper transition plate 8, spoke-type weight sensor 9, the lower transition plate 10, and the upper pressure head 12 are moved downwards, thus applying stress on the specimen of coal body 17.

2.1.3. Intermediate Principal Stress Applying System. As shown in Figure 2(a), the intermediate principal stress applying system consists mainly of a hydraulic oil cylinder 6, a piston rod 7, a lateral pressure head 14, a guide pressure block 15, two pressure blocks 16, and three nitrile rubbers 18. The nitrile rubber and the pressure block are alternately superimposed on the lateral pressure head, and the guide pressure block is located at the top, as seen in Figure 4. The guide pressure block, pressure block, nitrile rubber, and lateral pressure head as a whole unit apply the stress σ_2 on the coal specimen.

When applying the major principal stress, the upper pressure head 12 and the transfer pressure slider 11 move downward simultaneously, making both the coal specimen 17 and the nitrile rubber 18 shrink in the same amount. The upper pressure head 12 and the guide pressure block 15 always maintain a certain height difference, thus avoiding the interference with each other between the σ_1-direction pressure head and the σ_2-direction pressure head when applying σ_1 and σ_2.

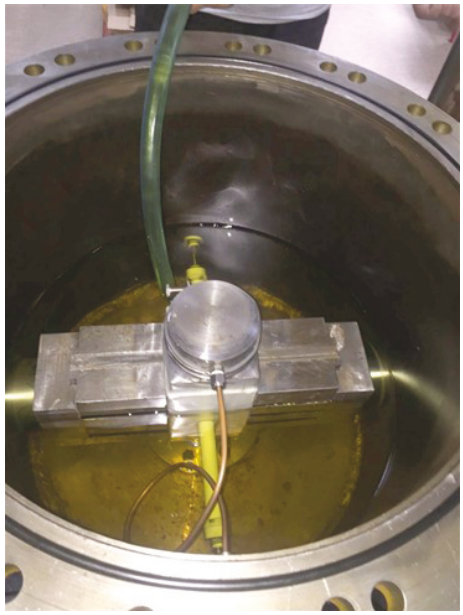

Figure 5: Photos of injecting hydraulic oil into the true triaxial pressure cell.

2.1.4. Minor Principal Stress Applying System. As shown in Figure 2(b), the σ_3-directional stress is applied to the coal specimen through high-pressure hydraulic oil. During the test, firstly, hydraulic oil is injected into the true triaxial pressure cell through the oil pump; after approximately full filling, the cylinder and cover of the true triaxial pressure chamber are fixed by bolts, then the metering pump of the hydraulic servo system continues to inject oil into the true triaxial pressure cell, making the pressure in the cylinder rise gradually, thus the stress in the σ_3-direction of coal specimen is applied. Figure 5 shows the photos of injecting hydraulic oil into the true triaxial pressure cell.

2.2. Hydraulic Servo System. The system is the power source of σ_1, σ_2, and σ_3. It is equipped with a set of high-pressure oil source and four independent sets of metering pumps with constant speed and constant pressure to provide σ_1, σ_2, and σ_3. A metering pump has a series of operational modes as the tracking mode, constant pressure mode, constant speed mode, manual mode, and position mode. The servo system can automatically control the pump's operation and ensure real-time acquisition of the technical parameters of the metering pump including pressure, flow, and in-pump and off-pump volumes. Figure 6 shows the metering pump for constant speed and constant pressure.

2.3. Gas Seepage System. The system consists of a high-pressure gas cylinder, a pressure-reducing valve, gas conduits, and other components. The test gas is introduced from the high-pressure gas cylinder, first entering the cylinder of the true triaxial pressure cell after passing in turn through the pressure-reducing valve, a gas conduit, the upper pressure head, and another gas conduit, then flowing over the coal specimen and out the lower pressure head, and last discharging to the outside after passing through the mass flow meter.

Figure 6: Metering pump for constant speed and constant pressure.

In order to tightly seal the rectangular cubic coal samples, a ring of circular groove is placed outside the honeycomb holes of the upper pressure head, and an O-ring sealing washer is placed into the groove to ensure gas tightness. In the experiment, the upper and lower pressure heads as well as the coal sample are bonded into a whole using No. 704 silica gel. Then, the whole package is fixed using the heat shrink tube, firmly fastened using the adjustable steel wire fastener, and installed into the true triaxial pressure cell. The seepage system can bear a maximum gas pressure of 3 MPa, as proven after a series of testing. Figure 7 shows a well-sealed and installed test piece.

2.4. Monitoring and Control System. The experimental data are measured using various precision sensors. σ_1 is detected using the spoke-type weight sensor. σ_2 and σ_3 are obtained using the pressure sensor and converted to standard electrical signals. The strain components ε_1 and ε_2 in the σ_1 and σ_2 directions are measured using the differential-transducer type high-precision displacement sensor, and the strain component ε_3 in the σ_3 direction is measured by the custom-built extensometer. The gas flow is measured by the high-pressure-resistant D07-11CM-type mass flow meter. The data measured using various sensors are sequentially sent to a computer, displayed, and stored using DHDAS software and analyzed using the DH5923 analysis system. Since the data are continuously and automatically collected, they are guaranteed to be reliable.

3. Materials and Methods

3.1. Materials and Sample Preparation. Coal samples were taken from N2808 Face of No. 8 Coalbed at Yuyang Coal Mine of Chongqing Songzao Coal & Electricity Co., Ltd. The coalbed, as the mainly mining coalbed of the coal mine, is a soft, medium thick one with average thickness of 2.4 m. The failure type of the original coal seam belongs to V class with gas content of 15.08~29.4 m^3/t, and gas permeability coefficient of 0.013 $m^2/(MPa^2 \cdot d)$. The coal mine has undergone multiple coal and gas outburst events with maximum strength up to 695 t.

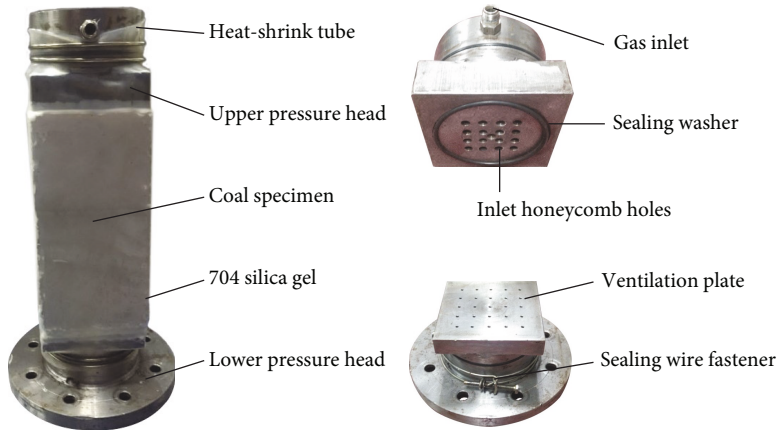

Figure 7: One well-sealed and installed test piece.

Table 1: Loading parameters.

Number	Preset σ_1 (MPa)	Preset σ_2 (MPa)	Preset σ_3 (MPa)	P (MPa)
1	4	4	4	
2	6	6	4	0.5
3	8	8	4	
4	4	4	4	
5	6	6	4	1.0
6	8	8	4	
7	4	4	4	
8	6	6	4	1.5
9	8	8	4	

The basic parameters of the coal seam are as follows: coal moisture content of 1.14%, dry ash basis of 15.23%, dry ash-free basis of 10.41%, consistent coefficient of 0.21–0.38, porosity of 9.48%, gas adsorption volume constant of 33.68 m^3 t^{-1}, and gas adsorption pressure constant of 1.25 MPa^{-1}.

Because No. 8 coal seam has a soft texture and is prone to fragility, the raw coal samples are very difficult to process. Thus, briquette samples were used in the experiment. Pulverized original coal samples were sieved to obtain a total of 2.55 kg equivalent coal powders of 20–40 meshes and 40–80 meshes. After being uniformly mixed with water, the coal powder mud was shaped in the specially designed specimen molds for 30 min at the shaped pressure of 100 MPa using a 100 t press and prepared as rectangular cubic samples of 100 mm × 100 mm × 200 mm in size. The processed samples were placed in an 80°C oven for 24 h and wrapped with plastic film for testing.

3.2. Experimental Design. The shear-seepage tests of coal under true triaxial stresses were performed using the true triaxial apparatus. First, the major, intermediate, and minor principal stresses σ_1, σ_2, and σ_3 were applied to the preset values and kept invariant. Then, gas was filled with inlet pressures of 0.5 MPa, 1 MPa, and 1.5 MPa. Once gas adsorption reached equilibrium, σ_1 was continuously applied to the specimen until it failed. Table 1 shows the loading parameters.

Figure 8: Specimens after shear seepage tests.

The permeability of the shale is continuously calculated as [40]

$$K = \frac{2q\mu LP_n}{A\left(P_1^{\,2} - P_2^{\,2}\right)}, \tag{1}$$

where K is the average permeability of gas (m^2), q is the velocity of gas seepage (m^3/s), μ is the dynamic viscosity coefficient of gas and usually taken as 1.087×10^{-11} MPa·s, L is the length of the coal sample (m), P_n is 1 atm, A is the cross-sectional area of the sample (m^2), P_1 is the pressure of gas at the inlet (MPa), and P_2 is the pressure of gas at the outlet (MPa).

4. Results and Discussion

Figure 8 shows the photos of briquette samples after being subjected to shear seepage tests. From the figure, it is clear that coal samples suffered significant shear failure under the action of true triaxial stresses, showing the shear planes with a 63° angle to the horizontal planes.

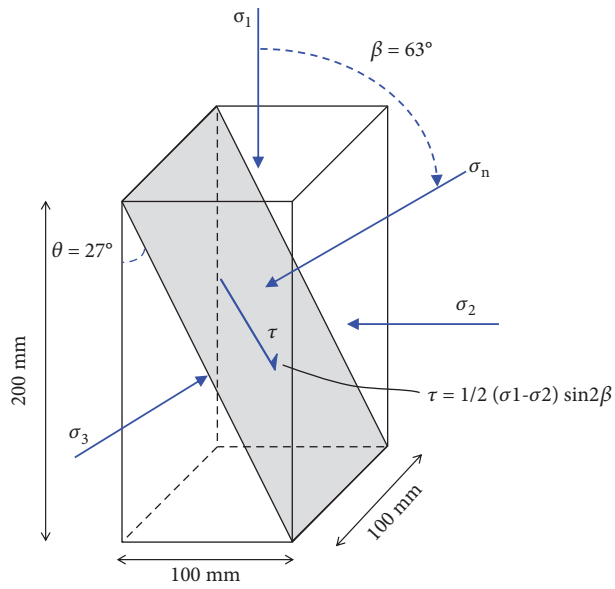

FIGURE 9: Shear stresses and shear displacement calculated from the applied major principal stress and intermediate principal stress.

Figure 9 shows the directions of the applied stresses with respect to the fracture orientation. The sliding direction is on the $\sigma_1 - \sigma_2$ plane, perpendicular to the σ_3 axis. As a result, the shear stress (τ) and shear displacement (d_s) can be determined as follows:

$$\tau = \frac{1}{2}(\sigma_1 - \sigma_2) \sin 2\beta, \tag{2}$$

$$d_s = \frac{1}{2}(d_1 - d_2) \sin 2\beta, \tag{3}$$

where σ_1 and σ_2 are the major and intermediate principal stresses, d_1 and d_2 are the specimen displacements monitored in the direction of σ_1 and σ_2, and β is the angle between σ_1 and σ_n directions. For all specimens, angle β equals to 63° and no shear stress on the $\sigma_2 - \sigma_3$ plane.

Figure 10 shows the shear stress-shear displacement-permeability curves of coal samples subject to different intermediate principal stresses and gas pressure. The following can be seen from the figure. First, the shear stress displays a nonlinear growth. The primary microscopic pores and fractures inside the coal specimen are gradually compacted to closure, leading to a decrease in porosity and gas seepage passageways. Therefore, the gas flow is blocked and gas permeability displays a gradual decreasing trend. Second, the shear stress approximately displays a linear growth. The primary microscopic pores and fractures are further compacted to closure, resulting in a further reduction in porosity and a continuous lowering in permeability. Then, the shear stress continues to increase, but its increasing rate gradually decreases. The specimen gradually begin to produce shear cracks. But because the shear cracks do not cut through, the gas seepage passageways continue to narrow down, further decreasing gas permeability to its minimum when reaching the peak shear strength. Last, the specimen is in the rapid stress falling stage, and the shear cracks gradually penetrate and form a macroscopic shear plane. The number of gas seepage passageways increases, leading to an upward trend in permeability. However, due to the squeezing, pressing, and dislocating of coal particles, gas seepage passageways are blocked or clogged, resulting in only a slight increase in permeability.

Figure 11 shows the changes of peak shear strength and initial gas permeability under different intermediate principal stress and gas pressure. It is obvious from the figure that the peak shear strength of coal specimen increases linearly with the increase in intermediate principal stress, while the initial gas permeability decreases linearly with the increase in intermediate principal stress. When the gas pressure is 0.5 MPa, with the intermediate principal stress increasing from 4 MPa to 6 MPa and 8 MPa, the corresponding peak shear strength increases from 6.58 MPa to 7.28 MPa and to 8.12 MPa and by 10.6% and 23.4%, respectively, and the initial permeability declines from 18.18×10^{-15} m^2 to 15.57×10^{-15} m^2 and 12.77×10^{-15} m^2, by 14.4% and 28.7%, respectively. When the gas pressure is 1.0 MPa, with the intermediate principal stress increasing from 4 MPa to 6 MPa and 8 MPa, the corresponding peak shear strength increases from 5.34 MPa to 6.24 MPa and 7.41 MPa, by 16.9% and 20.0%, respectively, and the initial permeability declines from 15.09×10^{-15} m^2 to 13.28×10^{-15} m^2 and 10.57×10^{-15} m^2, by 12.0% and 30.0%, respectively. When the gas pressure is 1.5 MPa, with the intermediate principal stress increasing from 4 MPa to 6 MPa and 8 MPa, the corresponding peak shear strength increases from 4.18 MPa to 5.42 MPa and to 6.26 MPa and by 29.7% and 49.8%, respectively, and the initial permeability decreases from 13.23×10^{-15} m^2 to 11.45×10^{-15} m^2 and 9.49×10^{-15} m^2, by 13.5% and 28.3%, respectively. Therefore, the greater the intermediate principal stress, the greater the coal's peak shear strength, and the smaller the initial gas permeability.

Figure 11 also shows that the gas pressure significantly affects coal's mechanical and seepage characteristics. When the intermediate principal stress and the minor principal stress are 4 MPa, with gas pressure increasing from 0.5 MPa to 1.0 MPa and 1.5 MPa, the coal's peak shear strength reduces from 6.58 MPa to 5.34 MPa and 4.18 MPa, by 18.8% and 36.5%, respectively, and the corresponding initial permeability declines from 18.18×10^{-15} m^2 to 15.09×10^{-15} m^2 and 13.23×10^{-15} m^2, by 17.0% and 27.2%, respectively. When the intermediate principal stress is 6 MPa and the minor principal stress is 4 MPa, with the gas pressure increasing from 0.5 MPa to 1.0 MPa and 1.5 MPa, the coal's peak shear strength decreases from 15.57 MPa to 13.28 MPa and 11.45 MPa, by 14.7% and 26.5%, respectively, and the corresponding initial permeability lowers from 15.57×10^{-15} m^2 to 13.28×10^{-15} m^2 and 11.45×10^{-15} m^2, by 14.7% and 26.5%, respectively. When the intermediate principal stress is 8 MPa and the minor principal stress is 4 MPa, with the gas pressure increasing from 0.5 MPa to 1.0 MPa and 1.5 MPa, the coal's peak shear strength decreases from 8.12 MPa to 7.41 MPa and 6.26 MPa, by 8.7% and

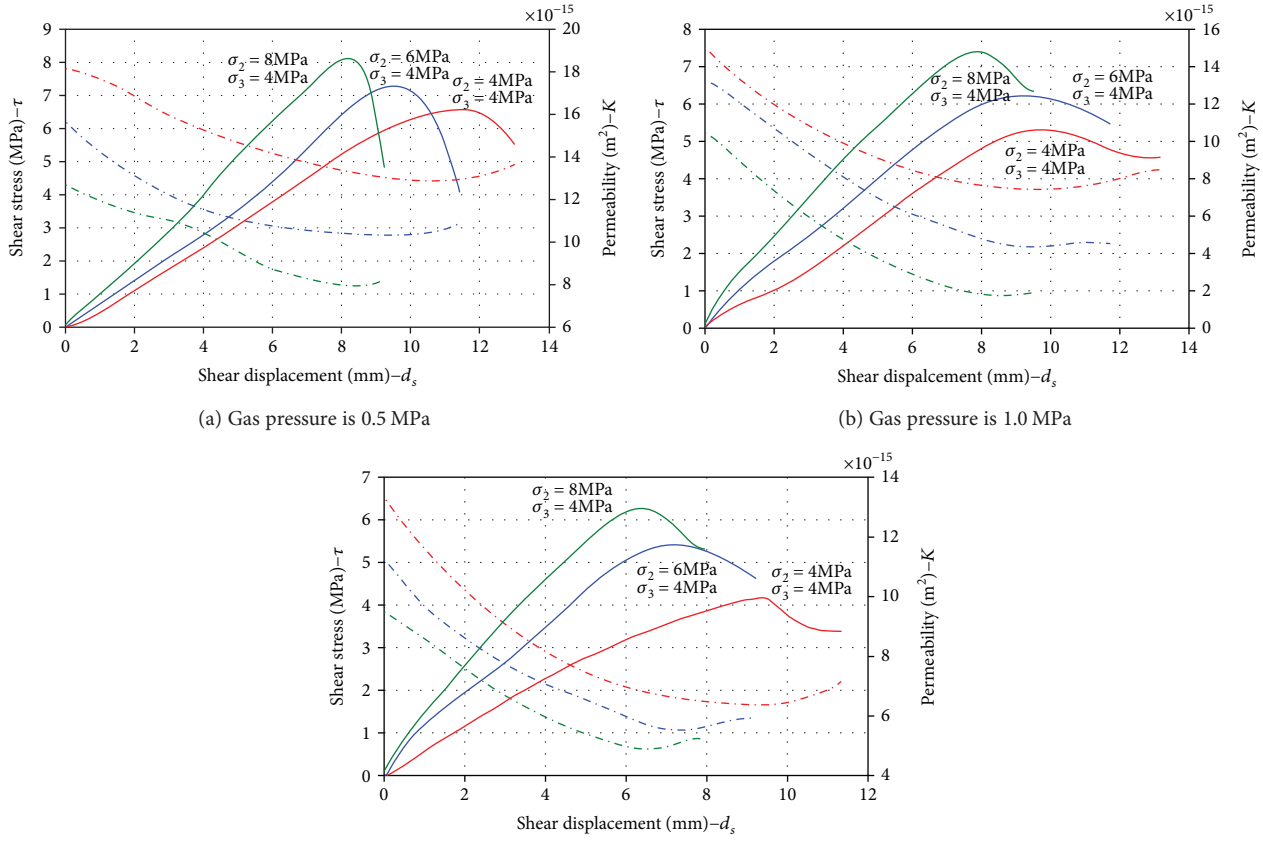

(a) Gas pressure is 0.5 MPa

(b) Gas pressure is 1.0 MPa

(c) Gas pressure is 1.5 MPa

FIGURE 10: The correlation curves of shear stress and permeability with intermediate principal stresses under different gas pressure conditions.

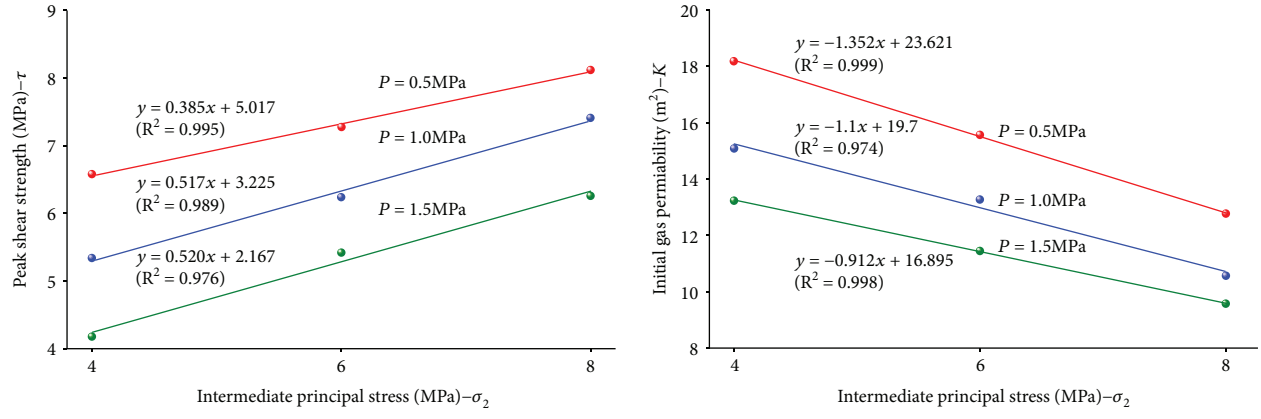

(a) The curves of peak shear strength with intermediate principal stress

(b) The curves of initial gas permeability with intermediate principal stress

FIGURE 11: The correlation curves of peak shear strength and initial gas permeability with intermediate principal stress under different gas pressure conditions.

22.9%, respectively, and the corresponding initial permeability reduces from 12.77×10^{-15} m^2 to 10.57×10^{-15} m^2 and 9.49×10^{-15} m^2, by 17.2% and 25.7%, respectively. Therefore, the greater the gas pressure is, the smaller the coal's peak shear strength and the initial permeability.

5. Conclusions

This paper particularly introduced a novel true triaxial apparatus and used it to study the characteristics of shear-seepage of coal under true triaxial stresses. The

apparatus can use its hydraulic servo system to independently provide three-dimensional stresses and have good air tightness and stable operational performance under gas pressure, making the study of shear-seepage properties under true triaxial stress conditions a reality. Under different intermediate principal stress conditions, the coal specimens were subjected to significant shear failure with the shear planes at the angle of 63°. The shear stress loading has gone through different stages, and the permeability increases slightly after rapidly and slowly decreasing and eventually reaching equilibrium. The greater the intermediate principal stress, the greater the coal's peak shear strength, and the smaller the initial gas permeability. The greater the gas pressure, the smaller the coal's peak shear strength and the initial permeability. The results demonstrate the effectiveness and reliability of the novel true triaxial apparatus.

Data Availability

The data used to support the findings of this study are available from the corresponding author upon request.

Conflicts of Interest

The authors declare that they have no conflicts of interest.

Acknowledgments

The authors would like to acknowledge the support of the National Natural Science Foundation of China (Project nos. 51304128, 51304237, and 51474106), the Specialized Research Fund for the Doctoral Program of Higher Education (Project no. 20133718120013), the Program for the Outstanding Young Scientists of Shandong University of Science and Technology (Project no. 2015JQJH105), the Taishan Scholar Talent Team Support Plan for Advantaged & Unique Discipline Areas, and the Source Innovation Program (Applied Research Special-Youth Special) of Qingdao (Project no. 17-1-1-38-jch).

References

[1] Q. T. Hu and G. C. Wen, *Mechanical Mechanism of Coal and Gas Outburst Process*, Science Press, Beijing, 2013.

[2] Q. T. Hu, S. N. Zhou, and X. Q. Zhou, "Mechanical mechanism of coal and gas outburst process," *Journal of China Coal Society*, vol. 33, no. 12, pp. 1368–1372, 2008.

[3] W. H. Somerton, I. M. Söylemezoğlu, and R. C. Dudley, "Effect of stress on permeability of coal," *International Journal of Rock Mechanics and Mining Sciences & Geomechanics Abstracts*, vol. 12, no. 5-6, pp. 129–145, 1975.

[4] S. Harpalani and R. Schraufnagel, "Shrinkage of coal matrix with release of gas and its impact on permeability of coal," *Fuel*, vol. 69, no. 5, pp. 551–556, 1990.

[5] G. Barla, M. Barla, and D. Debernardi, "New triaxial apparatus for rocks," *Rock Mechanics and Rock Engineering*, vol. 43, no. 2, pp. 225–230, 2010.

[6] J. Xu, S. J. Peng, G. Z. Yin, Y. Q. Tao, H. W. Yang, and W. Z. Wang, "Development and application of triaxial servo-controlled seepage equipment for thermo-fluid-solid coupling of coal containing methane," *Chinese Journal of Rock Mechanics and Engineering*, vol. 29, no. 5, pp. 907–914, 2010.

[7] P. G. Ranjith and M. S. A. Perera, "A new triaxial apparatus to study the mechanical and fluid flow aspects of carbon dioxide sequestration in geological formations," *Fuel*, vol. 90, no. 8, pp. 2751–2759, 2011.

[8] R. Shukla, P. G. Ranjith, S. K. Choi, and A. Haque, "A novel testing apparatus for hydromechanical investigation of rocks: geo-sequestration of carbon dioxide," *Rock Mechanics and Rock Engineering*, vol. 45, no. 6, pp. 1073–1085, 2012.

[9] M. S. A. Perera, P. G. Ranjith, and S. K. Choi, "Coal cleat permeability for gas movement under triaxial, non-zero lateral strain condition: a theoretical and experimental study," *Fuel*, vol. 109, pp. 389–399, 2013.

[10] B. Mishra and P. Verma, "Uniaxial and triaxial single and multistage creep tests on coal-measure shale rocks," *International Journal of Coal Geology*, vol. 137, no. 1, pp. 55–65, 2015.

[11] H.-D. Chen, C. Yuan-Ping, H.-X. Zhou, and W. Li, "Damage and permeability development in coal during unloading," *Rock Mechanics and Rock Engineering*, vol. 46, no. 6, pp. 1377–1390, 2013.

[12] Q. Liu, Y. Cheng, K. Jin, Q. Tu, W. Zhao, and R. Zhang, "Effect of confining pressure unloading on strength reduction of soft coal in borehole stability analysis," *Environmental Earth Sciences*, vol. 76, no. 4, p. 173, 2017.

[13] G. Wang, W. Li, P. Wang, X. Yang, and S. Zhang, "Deformation and gas flow characteristics of coal-like materials under triaxial stress conditions," *International Journal of Rock Mechanics and Mining Sciences*, vol. 91, no. 1, pp. 72–80, 2017.

[14] B. Haimson and C. Chang, "A new true triaxial cell for testing mechanical properties of rock, and its use to determine rock strength and deformability of Westerly granite," *International Journal of Rock Mechanics and Mining Sciences*, vol. 37, no. 1-2, pp. 285–296, 2000.

[15] A. D. Alexeev, V. N. Revva, N. A. Alyshev, and D. M. Zhitlyonok, "True triaxial loading apparatus and its application to coal outburst prediction," *International Journal of Coal Geology*, vol. 58, no. 4, pp. 245–250, 2004.

[16] L. Lombos, D. W. Roberts, and M. S. King, *Design and Development of Integrated True Triaxial Testing System*, True Triaxial Testing of Rocks. Taylor & Francis, London, 2013.

[17] L. P. Frash, M. Gutierrez, and J. Hampton, "True-triaxial apparatus for simulation of hydraulically fractured multiborehole hot dry rock reservoirs," *International Journal of Rock Mechanics and Mining Sciences*, vol. 70, pp. 496–506, 2014.

[18] M. H. B. Nasseri, S. D. Goodfellow, L. Lombos, and R. P. Young, "3-D transport and acoustic properties of fontainebleau sandstone during true-triaxial deformation experiments," *International Journal of Rock Mechanics and Mining Sciences*, vol. 69, pp. 1–18, 2014.

[19] M. C. He, F. Zhao, M. Cai, and S. Du, "A novel experimental technique to simulate pillar burst in laboratory," *Rock Mechanics and Rock Engineering*, vol. 48, no. 5, pp. 1833–1848, 2015.

[20] X. T. Feng, X. Zhang, R. Kong, and G. Wang, "A novel mogi type true triaxial testing apparatus and its use to obtain complete stress-strain curves of hard rocks," *Rock Mechanics and Rock Engineering*, vol. 49, no. 5, pp. 1649–1662, 2016.

[21] M. H. Li, G. Z. Yin, J. Xu, W. P. Li, Z. L. Song, and C. B. Jiang, "A novel true triaxial apparatus to study the geomechanical and fluid flow aspects of energy exploitations in geological formations," *Rock Mechanics and Rock Engineering*, vol. 49, no. 12, pp. 4647–4659, 2016.

[22] K. Mogi, "Effect of the intermediate principal stress on rock failure," *Journal of Geophysical Research*, vol. 72, no. 20, pp. 5117–5131, 1967.

[23] K. Mogi, "Fracture and flow of rocks under high triaxial compression," *Journal of Geophysical Research*, vol. 76, no. 5, pp. 1255–1269, 1971.

[24] M. Takahashi and H. Koide, "Effect of the intermediate principal stress on strength and deformation behavior of sedimentary rocks at the depth shallower than 2000 m," in *ISRM International Symposium*, Pau, France, August-September 1989.

[25] G. Z. Yin, J. Lu, X. Li, G. Bian, Z. L. Song, and Y. B. Liu, "Influence of intermediate principal stress on dilation and strength characteristics of sandstone," *Journal of China Coal Society*, vol. 42, no. 4, pp. 879–885, 2017.

[26] M. H. Li, G. Z. Yin, J. Xu, J. Cao, and Z. L. Song, "Permeability evolution of shale under anisotropic true triaxial stress conditions," *International Journal of Coal Geology*, vol. 165, no. 8, pp. 142–148, 2016.

[27] I. W. Yeo, M. H. de Freitas, and R. W. Zimmerman, "Effect of shear displacement on the aperture and permeability of a rock fracture," *International Journal of Rock Mechanics and Mining Sciences*, vol. 35, no. 8, pp. 1051–1070, 1998.

[28] K. J. Shou and Y. W. Lin, "Design and verification of portable direct shear tester with application to remolded colluvium geomaterials," *Journal of Rock Mechanics and Geotechnical Engineering*, vol. 4, no. 4, pp. 326–332, 2012.

[29] N. Barton, "Shear strength criteria for rock, rock joints, rockfill and rock masses: problems and some solutions," *Journal of Rock Mechanics and Geotechnical Engineering*, vol. 5, no. 4, pp. 249–261, 2013.

[30] P. Kapang, C. Walsri, T. Sriapai, and K. Fuenkajorn, "Shear strengths of sandstone fractures under true triaxial stresses," *Journal of Structural Geology*, vol. 48, no. 3, pp. 57–71, 2013.

[31] S. Thirukumaran and B. Indraratna, "A review of shear strength models for rock joints subjected to constant normal stiffness," *Journal of Rock Mechanics and Geotechnical Engineering*, vol. 8, no. 3, pp. 405–414, 2016.

[32] N. J. F. Koupouli, T. Belem, P. Rivard, and H. Effenguet, "Direct shear tests on cemented paste backfill-rock wall and cemented paste backfill-backfill interfaces," *Journal of Rock Mechanics and Geotechnical Engineering*, vol. 8, no. 4, pp. 472–479, 2016.

[33] F. Z. Meng, H. Zhou, Z. Q. Wang et al., "Experimental study on the prediction of rockburst hazards induced by dynamic structural plane shearing in deeply buried hard rock tunnels," *International Journal of Rock Mechanics and Mining Sciences*, vol. 86, no. 7, pp. 210–223, 2016.

[34] G. Wang, Y. J. Jiang, W. M. Wang, and Y. C. Li, "Development and application of an improved numeric control shear-fluid coupled apparatus for rock joint," *Rock and Soil Mechanics*, vol. 30, no. 10, pp. 3200–3208, 2009.

[35] J. Xu, H. Y. Tan, L. Wang, L. F. Lu, and H. Wu, "Meso-evolution process of gas-containing coal shear failure under different normal stresses," *Chinese Journal of Rock Mechanics and Engineering*, vol. 31, no. 6, pp. 1192–1197, 2012.

[36] R. Singh, M. Sivaguru, G. A. Fried et al., "Real rock-microfluidic flow cell: a test bed for real-time in situ analysis of flow, transport, and reaction in a subsurface reactive transport environment," *Journal of Contaminant Hydrology*, vol. 204, pp. 28–39, 2017.

[37] L. Wang, E. Parsa, Y. Gao et al., "Experimental study and modeling of the effect of nanoconfinement on hydrocarbon phase behavior in unconventional reservoirs," in *SPE Western North American and Rocky Mountain Joint Meeting*, Denver, CO, USA, April 2014.

[38] M. K. Shah, R. Fisher, I. Hassan, E. Makarov, and O. Medvedev, "Measuring reservoir fluid composition using a novel continuous contact flash method based on a microfluidic device," in *Abu Dhabi International Petroleum Exhibition and Conference*, Abu Dhabi, UAE, November 2015.

[39] W. Yun, C. M. Ross, S. Roman, and A. R. Kovscek, "Creation of a dual-porosity and dual depth micromodel for the study of multiphase flow in complex porous media," *Lab on a Chip*, vol. 17, no. 8, pp. 1462–1474, 2017.

[40] A. Hildenbrand, S. Schlomer, and B. M. Krooss, "Gas breakthrough experiments on fine-grained sedimentary rocks," *Geofluids*, vol. 2, no. 1, 23 pages, 2002.